

Article

Molecularly Engineered Lithium–Chromium Alkoxide for Selective Synthesis of LiCrO_2 and Li_2CrO_4 Nanomaterials

Olusola Ojelere , David Graf  and Sanjay Mathur *

Faculty of Mathematics and Natural Sciences, Institute of Inorganic Chemistry, University of Cologne, Greinstraße 6, D-50939 Cologne, Germany; ojelere@smail.uni-koeln.de (O.O.); dgraf@smail.uni-koeln.de (D.G.)

* Correspondence: sanjay.mathur@uni-koeln.de

Received: 11 January 2019; Accepted: 10 February 2019; Published: 14 February 2019



Abstract: Achieving control over the phase-selective synthesis of mixed metal oxide materials remains a challenge to the synthetic chemist due to diffusion-driven growth, which necessitates the search for new compounds with pre-existent chemical bonds between the phase-forming elements. We report here a simple solvothermal process to fabricate LiCrO_2 and Li_2CrO_4 nanoparticles from bimetallic single-source precursors, demonstrating the distinctive influence of molecular design and calcination conditions on the resulting nanomaterials. The chemical identity of $[\text{Li}_2\text{Cr}(\text{O}^t\text{Bu})_4\text{Cl}(\text{THF})_2]$ (**1**) and $[\text{LiCr}(\text{O}^t\text{Bu})_2(\text{PyCH}=\text{COCF}_3)_2(\text{THF})_2]$ (**2**) was unambiguously established in the solid state by single-crystal X-ray diffraction, revealing the formation of a coordination polymeric chain in compound **1**, whereas electron paramagnetic resonance spectroscopy (EPR) studies revealed a monomeric structure in solution. TEM analysis of synthesized LiCrO_2 nanoparticles showed nearly uniform particles size of approximately 20 nm. The sensitivity of the LiCrO_2 phase towards oxidation was investigated by X-ray diffraction, revealing the formation of the stable Li_2CrO_4 after calcination in air.

Keywords: heterometallic; heteroarylalkenol; precursors; solvothermal; nanoparticles

1. Introduction

The chemical synthesis of two-dimensional transition metal oxides has attracted considerable research attention due to their interesting physical, chemical, and electronic properties [1]. In particular, LiCrO_2 with a layered triangular arrangement of Cr^{3+} exhibits antiferromagnetic nature with two-dimensional (2D) frustration and interesting structural and magnetic behavior [2,3]. In general, geometrically frustrated magnetic materials are being widely studied, possibly due to their natural inclination towards unconventional ground states, which often leads to a suppression of long-range magnetic ordering and promotes short-range magnetic correlations owing to fluctuations between nearly or totally degenerated magnetic ground states [4,5]. Moreover, in lithium-ion batteries, the cathode materials are mostly layered compounds of lithium transition metal oxides (LiMO_2 , where $M = \text{V}, \text{Cr}, \text{Mn}, \text{Fe}, \text{Co}, \text{Ni}$, etc.), among which Cr-based cathode materials have attracted significant attention due to possible multiple electron transfer pathways and stable cyclability, which results from the three-electron redox couple $\text{Cr}^{3+}/\text{Cr}^{6+}$ [6–9]. The growing interest in the synthesis of lower-valency chromium complexes is due to their potential applications as catalysts in ring-opening polymerization reactions and as precursors for corresponding metal oxides [10,11]. However, only a few chromium(III) alkoxides are known, and their reactivity and structural patterns are not well established [12–16]. To our best knowledge, there is no report on the preparation of stoichiometric LiCrO_2 nanomaterials from molecular single-source precursors [17–19].

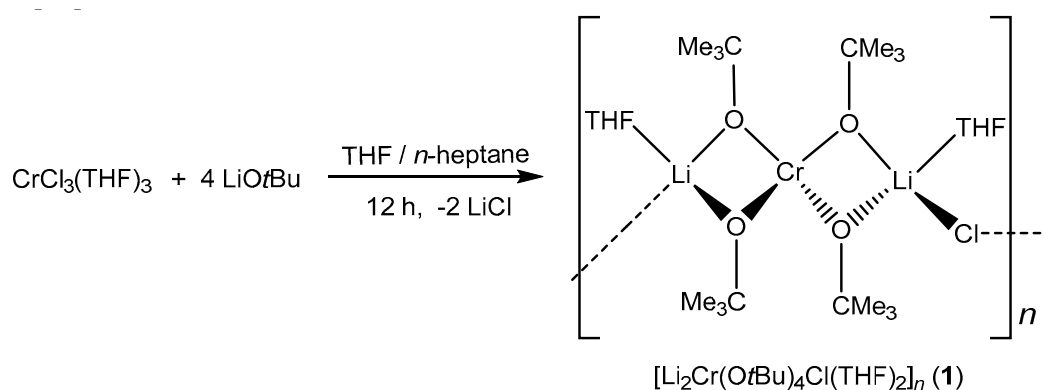
The pre-existent chemical bonds between the phase-forming elements in molecular precursors can facilitate the crystallization of materials at relatively lower temperature when compared to solid-state synthesis [20–22].

We demonstrate here, for the first time, the influence of molecular-level processing in the controlled synthesis of LiCrO₂ nanomaterials with stoichiometry control between the heterometallic precursors and the resulting mixed oxide ceramics, which is rather difficult in preparation with the solid-state or multi-source precursor approach.

2. Results and Discussion

2.1. Synthesis of [Li₂Cr(O^{*t*}Bu)₄Cl(THF)₂]_{*n*} (**1**)

The heterometallic alkoxide [Li₂Cr(O^{*t*}Bu)₄Cl(THF)₂] (**1**) was synthesized via a salt metathesis reaction between solvated CrCl₃ activated in THF (CrCl₃(THF)₃) and four equivalents of LiO^{*t*}Bu in THF/*n*-heptane (Scheme 1). The color of the reaction mixture changed from pale blue to purple after 12 h of stirring at room temperature. The excess solvent was removed under vacuum, and the resulting product was purified by washing with *n*-heptane. The obtained product was the chloride-containing compound [Li₂Cr(O^{*t*}Bu)₄Cl(THF)₂]_{*n*} (**1**) that forms a one-dimensional polymeric chain in the solid-state as revealed by single-crystal X-ray structure analysis. Elemental analysis showed deviations of carbon (found: 50.93%, calc.: 53.58%), possibly due to partial hydrolysis during the sample preparation.



Scheme 1. Synthesis of bimetallic lithium–chromium(III) compound **1**.

2.1.1. X-ray Crystallography of Compound **1**

The bimetallic lithium–chromium(III) compound **1** was isolated in THF at $-18\text{ }^\circ\text{C}$ and crystallized in the monoclinic space group *C2/c* with four molecules per unit cell. The asymmetric unit of compound **1** as shown in Figure 1 consisted of a trinuclear framework with the central chromium(III) atom adopting a distorted tetrahedral coordination sphere with four *tert*-butoxy ligands bridged to two peripheral lithium atoms. The bond distances between chromium and oxygen observed in compound **1** were 1.862 and 1.871 Å, respectively. The bond angles around the oxygen of the *tert*-butoxy ligand and chromium center were 83.03° and 124.56°, which deviates from ideal tetrahedral geometry (109.5°) due to the steric demand of the *tert*-butoxy groups. The peripheral lithium atoms were coordinated in a tetrahedral fashion by an additional THF and a chloride ligand per lithium atom. Moreover, the observed lithium–oxygen (Li–O) distances of 1.924 and 1.947 Å between the lithium center and the *tert*-butoxy ligand were shorter than the 1.963 Å observed between the lithium center and coordinating THF molecule, while the Li–Cl distance was 2.286 Å. The one-dimensional polymeric chain resulted from the Li–Cl–Li connection between the trinuclear asymmetric units. [Li₂Cr(O^{*t*}Bu)₄Cl(THF)₂] (**1**) is isostructural to the mixed iron(III)/lithium bromo alkoxide reported by Barley et al. [23] and Mantymaki et al [24]. The structure can be fully described with the formula

catena-poly[[tetra- μ_2 -*tert*-butoxo-1:2 κ^4 O:O;1:3 κ^4 O:O-bis(tetrahydrofuran)-2 κ O,3 κ O-chromium(III)-dilithium(I)]- μ -chloro].

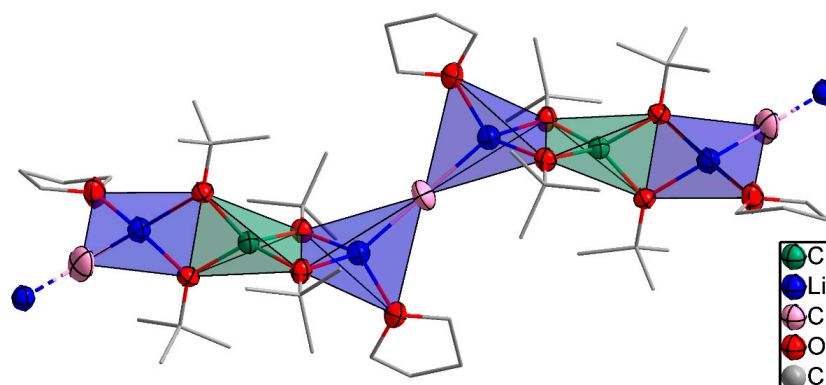


Figure 1. An illustration of the propagation of compound **1** to form polymeric chains. Thermal ellipsoids for Li, Cr, and O atoms are shown at the 50% probability level, and the H atoms have been omitted for the sake of clarity.

2.1.2. Electron Paramagnetic Resonance Spectroscopy (EPR) of Compound **1**

Electron paramagnetic resonance spectroscopy (EPR) of the synthesized complex was measured on the X-band using a 2,2-diphenyl-1-picrylhydrazyl (DPPH) reference. The EPR spectrum of compound **1** showed one broad resonance apparently resulting from the presence of a mononuclear chromium(III) species ($S = 3/2$, d^3) in solution and exhibited a Landé factor $g(\text{iso})$ of 1.972. The little hyper-fine coupling observed in the spectra could be attributed to the less-abundant chromium isotope ^{53}Cr with $I = 3/2$ (9.5% nat. abundance, Figure 2 inset). The feature at around 3388 G is reflected in the smaller feature at ~ 3416 G for the outer lines of the quartet resonance signal, where the inner lines overlap with the main signal, giving an estimated hyper-fine coupling of about 7 G for the ^{53}Cr isotopomer. The g -values observed in this compound were in good relation to the isotropic values reported for chromium(III) which are between 1.960 and 2.000 [25]. The influence of the two connected lithium centers to the hyperfine coupling of the chromium cation and the alkoxy ligands were not observed in the spectra. The UV–Vis spectra (Supplementary Materials, Figure S1) showed three absorption maxima at 406, 802, and an intense one at 610 nm resulting from the d–d transitions of the tetrahedral coordinated chromium(III) center.

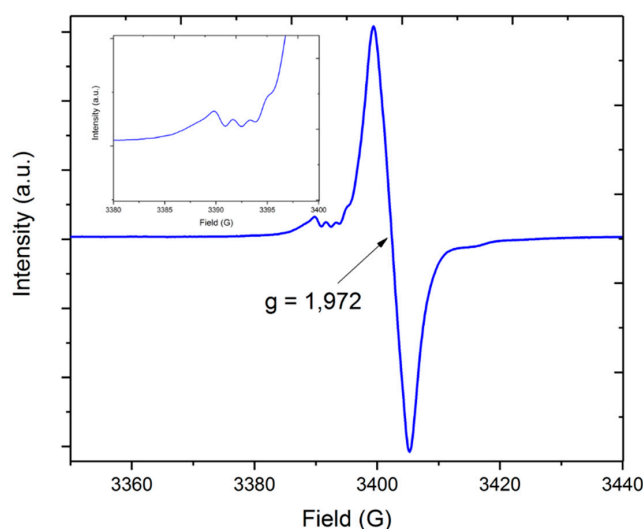
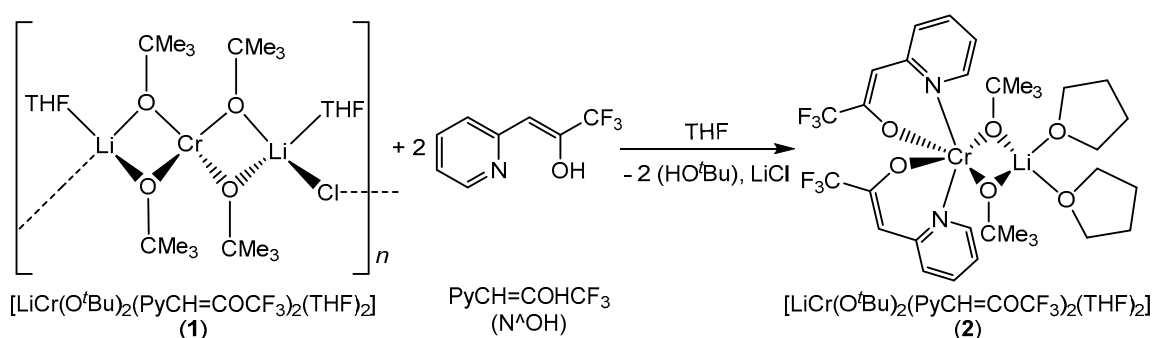


Figure 2. Electron paramagnetic resonance spectra of $[\text{Li}_2\text{Cr}(\text{O}^t\text{Bu})_4\text{Cl}(\text{THF})_2]$ (**1**) measured at room temperature in toluene.

2.2. Synthesis of $[\text{LiCr}(\text{O}^t\text{Bu})_2(\text{PyCH}=\text{COCF}_3)_2(\text{THF})_2]$ (2)

Mixed metal alkoxides are potential precursors to oxide ceramics due to their susceptibility to water that facilitates their hydrolytic activation and conversion into chemically homogeneous amorphous ceramics [26]. However, the limited thermal stability and extreme sensitivity of heterometallic alkoxides to moisture and air make their handling and storage rather difficult. Therefore, in our effort to improve the stability of compound 1, a ligand-modified alkoxide with enhanced stability was synthesized by adding two equivalents of bidentate β -heteroarylalkenol ligand 3,3,3-trifluoro(pyridin-2-yl)propen-2-ol ($\text{PyCH}=\text{COHCF}_3$) to the solution of compound 1 (Scheme 2). Upon the ligand addition, the color of the reaction mixture changed from purple to light-brown. The resulted compound 2 could be recrystallized from THF at -18°C . The single crystal X-ray diffraction showed a chromium(III) center in octahedral geometry with two β -heteroarylalkenol ligands and two *tert* butoxy groups shared between chromium and lithium centers. This compound showed higher stability in air due to good electron donating and accepting properties of the chelating ligands that provide both structural stability and electronic saturation around the chromium center [27]. The elemental analysis of the bulk material showed small deviations and revealed the selective transformation to the heteroleptic lithium–chromium complex.



Scheme 2. Synthesis of chelate ligand-modified bimetallic lithium–chromium(III) compound 2.

2.2.1. X-ray Crystallography of Compound 2

Compound 2 in Figure 3 crystallized in the monoclinic space group $P2_1/c$ with four molecules per unit cell. The nitrogen atoms of the bidentate ligands adopted the axial position with a steric distortion (170.74° against 180°), whereas the bond distances of Cr–N1 and Cr–N2 were 2.111 and 2.087 Å, respectively. The bond angles N1–Cr–O3 and N2–Cr–O1 of the two bidentate ligands were 85.18° and 84.31° , respectively, due to the constrained bite angle. Moreover, the equatorial Cr–O bond distances of the heteroarylalkenolate ligands were elongated (Cr1–O1: 1.971 Å) compared to the bridged alkoxo ligands (Cr1–O2: 1.950 Å). In the case of the tetrahedrally coordinated lithium center, the Li–O distances of the *tert*-butoxy ligand (Li1–O2: 1.912 Å) were shorter than the weakly coordinated THF molecule (Li1–O5: 2.007 Å).

The UV–Vis spectra showed an intense absorption maximum at 590 nm of the d–d transition and three weak maxima at 375, 306, and 270 nm resulting from the ligand-to-metal charge transfer (LMCT) and π – π^* transition of the aromatic moiety in the ligand backbone (Supplementary Materials, Figure S1). The bidentate ligand with the synergistic effect of the electron-donating aromatic system and the electron-pulling perfluoroalkyl-group stabilize the compound by a pseudo push–pull effect, which provides more stability to the molecule by saturating the coordination sphere of the chromium(III) center. However, compound (2) is not stable in the gas phase due to the weakly bonded THF molecules which were released before the sublimation point.

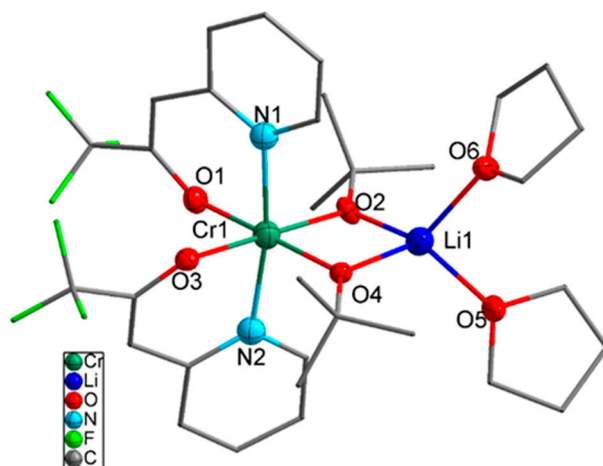


Figure 3. Molecular structure of compound 2. Thermal ellipsoids for Li, Cr, N, and O atoms are shown at the 50% probability level, and the H atoms have been omitted for clarity.

2.2.2. Thermogravimetric Analysis (TGA) of Compounds 1

Thermogravimetric analysis (TGA) of compound 1 was conducted from room temperature to 800 °C under a constant flow of nitrogen, and displayed a two-step decomposition profile (Figure 4). In the first step from 70 to 310 °C of the thermal transformation, a slow mass loss of around 25% was observed and it could be attributed to the release of weakly bonded two THF molecules. The sharp mass loss at a temperature of approximately 310 °C down to 28% of the initial mass owing to decomposition of *tert*-butoxy group from the complex indicated the formation of LiCrO_2 and LiCl , since the theoretical value of the residual mass is 25%. The slightly higher mass of the residue (3%) could be possibly due to carbon or fluorine impurities originating from the ligands.

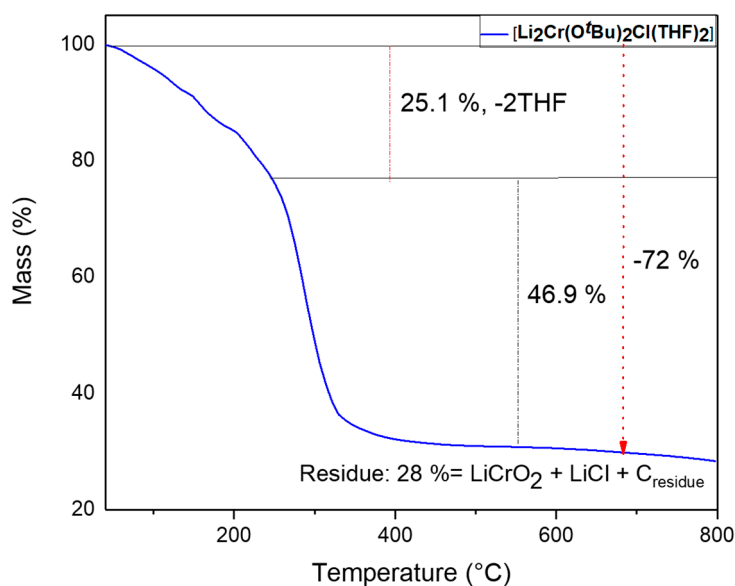


Figure 4. Thermogravimetric profile of compound 1.

2.3. Material Synthesis

The fabrication of LiCrO_2 nanoparticles was performed via solvothermal process using compound 2 in toluene under inert atmosphere with polyvinylpyrrolidone (PVP) as surfactant to influence the morphology of the formed oxide materials. A similar synthetic procedure was followed to synthesize Li_2CrO_4 using compound 1 which contained Li–Cr in a 2:1 ratio. As already explained by TGA, compound one can also be utilized as a precursor to LiCrO_2 and LiCl , as the byproduct is

soluble in water and can be removed during purification of the nanoparticle by washing with water before calcination.

The powder X-ray pattern of the solid product obtained from compound **2** revealed the formation of crystalline LiCrO_2 (JCPDS 24-0600) [28] with some unidentified (amorphous) component (Figure 5). The material obtained from compound **1** containing Li–Cr in a 2:1 ratio was found to be Li_2CrO_4 (JCPDS 31-0715) [29].

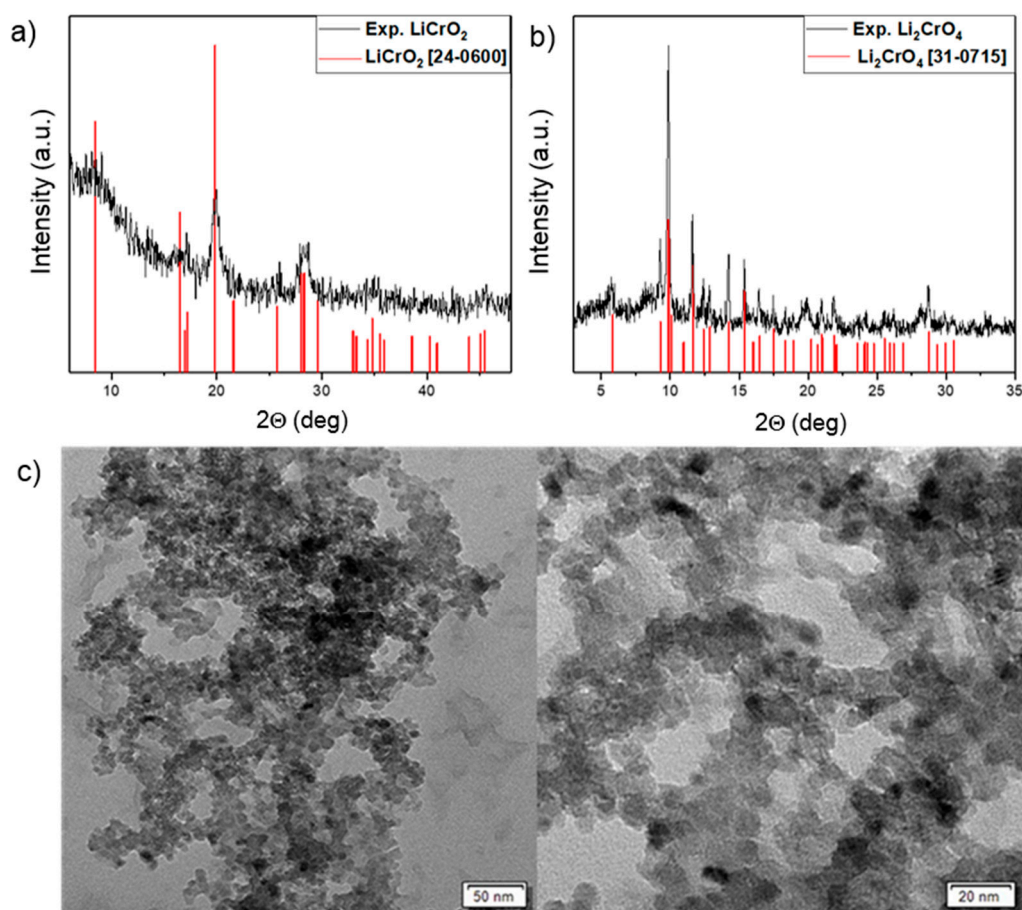


Figure 5. (a) XRD pattern of LiCrO_2 nanoparticles. (b) XRD pattern of Li_2CrO_4 nanoparticles. (c) TEM images of LiCrO_2 nanoparticles.

The structural features of the prepared LiCrO_2 nanoparticles were observed by transmission electron microscope (TEM), which showed nearly uniform grains with particles of average size 20 nm (Figure 5). However, some agglomeration was observed due to residual carbon or surfactant (PVP).

The previously reported multi-source synthesis of LiCrO_2 resulted in inhomogeneous elemental distribution and nonuniform morphologies, which could be detrimental to application of the material. For instance, the report of Tanaka et al. for the synthesis of lithium chromium oxide nanoparticles by induction thermal plasmas resulted in material with different oxide phases and inhomogeneous morphology [30]. Therefore, synthesizing LiCrO_2 nanomaterials from single-source precursors **1** and **2** is a promising strategy to impose a better phase control (Figure 6).

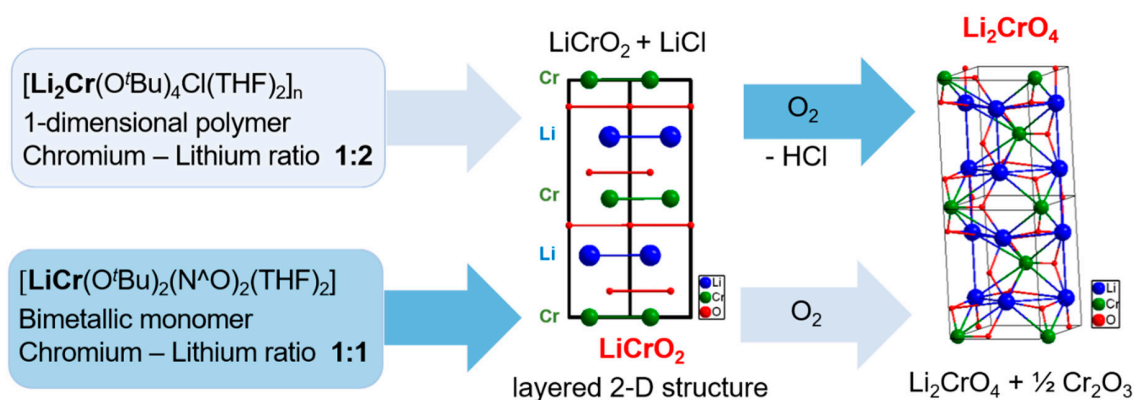


Figure 6. Illustration of the phase-selective transformations of compound 1 to Li_2CrO_4 and compound 2 to LiCrO_2 .

3. Materials and Methods

All syntheses were performed under an inert nitrogen atmosphere using a modified Stock glass vacuum line. The used solvents were dried and distilled over sodium and stored over molecular sieves. All chemicals were of analytical grade and used without further purification. Chromium(III) chloride (CrCl_3) was obtained from Acros Organics (97% purity, Morris Plains, NJ, USA) and activated in dried THF by stirring for one day at room temperature. X-band EPR spectra were recorded with a Bruker System ELEXSYS 500E instrument (Bruker, Karlsruhe, Germany equipped with a Bruker ER 4131VT variable-temperature unit). Single-crystal XRD analysis and structure elucidation was performed on a STOE IPDS II diffractometer (STOE, Darmstadt, Germany) with graphite monochromated $\text{Mo K}\alpha$ radiation (0.71071 Å). A numerical absorption correction based on crystal shape optimization was applied for all data. The programs used in this work were *STOE's XAREA* [31–33] and the *WINGX* suite of programs [34], including *SIR-92* [35], *SHELX*, and *SHELXTL* [36], and *PLATON* [37] for structure solution and refinement. H atoms were calculated geometrically, and a riding model was applied during the refinement process. Powder X-ray diffraction measurements were performed on a STOE-STADI P using $\text{Mo K}\alpha$ radiation (0.71071 Å). TEM measurement was carried out by a TEM LEO912 omega from Zeiss company (Oberkochen, Germany) operated at 120 kV.

3.1. Precursor Synthesis

$[\text{Li}_2\text{Cr}(\text{O}^t\text{Bu})_4\text{Cl}(\text{THF})_2]_n$ (**1**): A solution of (1.00 g, 6.31 mmol) CrCl_3 activated in 50 mL THF was slowly added to a solution containing four equivalent of $[\text{Li}(\text{O}^t\text{Bu})]$ (1.52 g, 18.94 mmol) in 20 ml *n*-heptane/THF to afford a pale blue solution which later changed to purple after stirring for 12 h at room temperature. Volatile solvent was removed under vacuum and the resulting product was extracted from an *n*-heptane solution to get rid of the LiCl. A single-crystal was obtained from a concentrated solution in THF/*n*-heptane. The obtained yield was 73% (2.48 g, 4.61 mmol) of a purple solid. Elemental analysis expected: C: 53.58, H: 9.74, found: C: 50.93, H: 10.02.

$[\text{LiCr}(\text{O}^t\text{Bu})_2(\text{PyCH}=\text{COCF}_3)_2(\text{THF})_2]$ (**2**): A solution of 3,3,3-trifluoro(pyridin-2-yl) propen-2-ol ($\text{PyCH}=\text{COHCF}_3$) (0.71 g, 3.76 mmol) in 10 ml THF was slowly added to a purple solution of $[\text{Li}_2\text{Cr}(\text{O}^t\text{Bu})_4\text{Cl}(\text{THF})_2]$ (**1**) (1.00 g, 1.86 mmol) in 10 mL THF and stirred for 2 h at room temperature. Volatile solvent was removed under vacuum, and the resulting product was extracted from THF/*n*-heptane solution. The obtained yield was 91% (1.23 g, 1.69 mmol) of a light brown solid. Elemental analysis expected: C: 52.97, H: 6.11 and N: 3.86, found: C: 52.02, H: 6.16 and N: 3.53.

Single-crystals were obtained from a mixture *n*-heptane and THF solution at -18°C . Compound **2** crystallized as a merohedric twin and was solved using twin law.

3.2. Synthesis of LiCrO₂ Nanoparticles

LiCrO₂ nanoparticles were prepared by dissolving 1.08 g of the precursor [LiCr(O^tBu)₂(PyCH=COCF₃)₂(THF)₂] (**2**) in 20 ml toluene and stirring until a uniform solution was obtained, followed by the addition of 0.3 g of poly(vinylpyrrolidone) (PVP; MW = 1,300,000) in isopropanol and magnetically stirred for 2 h to obtain a homogeneous solution. The mixture was then transferred into a Teflon-lined stainless-steel autoclave and heated at 180 °C for 24 h. Finally, the obtained precipitates were centrifuged, collected, and rinsed with deionized water and ethanol five times, and then dried at 70 °C under vacuum overnight. The dried nanoparticles were then calcinated at 600 °C for 2 h in nitrogen atmosphere to produce LiCrO₂ nanoparticles.

3.3. Synthesis of Li₂CrO₄ Nanoparticles

Li₂CrO₄ nanoparticles were prepared in a similar procedure as described above for LiCrO₂ nanoparticles. However, the obtained material was calcinated in air for 5 h to remove the leftover PVP from the material during which the material was oxidized from (III) to (IV).

4. Conclusions

In this study, a facile and efficient solvothermal method was employed to fabricate LiCrO₂ and Li₂CrO₄ nanoparticles from new heterometallic chromium(III)-based alkoxide, which was successfully stabilized via ligand modification using 3,3,3-trifluoro(pyridin-2-yl) propen-2-ol (PyCH=COCF₃). The strategy behind the synthesis of the precursors was to provide precise control over material stoichiometry at the molecular level, which is challenging in traditional solid-state synthesis. Since chromium is an earth-abundant element, its complexes and oxide materials can serve as economical and sustainable materials for device applications.

Supplementary Materials: The following are available online at <http://www.mdpi.com/2304-6740/7/2/22/s1>, Table S1: Details on crystal and structure refinement of compound **1**, Table S2: Selected bond distances (Å) of compounds **1**, Table S3: Selected bond angles (°) of compound **1**, Table S4: Details on crystal and structure refinement of compound **2**, Table S5: Selected bond distances (Å) of compound **2**, Table S6: Selected bond angles (°) of compound **2**, Figure S1: UV-vis spectra of compound **1** and **2**. Additional details concerning the structure determination are available in CIF format and have been deposited under the CCDC entry numbers 1896969 for [Li₂Cr(O^tBu)₄Cl(THF)₂]*n* (**1**) and 1890295 for [LiCr(O^tBu)₂(PyCH=COCF₃)₂(THF)₂] (**2**). Copies of the data can be obtained free of charge from CCDC (<http://www.ccdc.cam.ac.uk/conts/retrieving.html>). CIF and CheckCIF are included in the Supplementary Materials.

Author Contributions: Study design, investigation, and preparation of manuscript were carried out by O.O. and D.G.; supervision and reviewing by S.M.

Funding: This research was funded by German Academic Exchange Service (DAAD), grant number 91563589 and University of Cologne.

Acknowledgments: The authors are grateful for the financial support provided by the University of Cologne and German Academic Exchange Service (DAAD) for doctoral scholarship provided to Olusola Ojelere with award No: 91563589. Additionally, special thanks are due to Ingo Pantenburg, Aaron Sandleben, Markus Schuetz, Thomas Fischer, and Nurgül Tosun for single-crystal, EPR, TGA, and TEM measurement, respectively.

Conflicts of Interest: The authors declare no conflicts of interest.

References

1. Wang, L.; Hu, P.; Long, Y.; Liu, Z.; He, X. Recent advances in ternary two-dimensional materials: Synthesis, properties and applications. *J. Mater. Chem. A* **2017**, *5*, 22855–22876. [CrossRef]
2. Li, G.; Höpfner, P.; Schäfer, J.; Blumenstein, C.; Meyer, S.; Bostwick, A.; Rotenberg, E.; Claessen, R.; Hanke, W. Magnetic order in a frustrated two-dimensional atom lattice at a semiconductor surface. *Nat. Commun.* **2013**, *4*, 1620. [CrossRef] [PubMed]
3. Mazin, I.I. Electronic structure and magnetism in the frustrated antiferromagnet LiCrO₂: First-principles calculations. *Phys. Rev. B* **2007**, *75*, 094407. [CrossRef]

4. Alexander, L.K.; Büttgen, N.; Nath, R.; Mahajan, A.V.; Loidl, A. ^7Li NMR studies on the triangular lattice system LiCrO_2 . *Phys. Rev. B* **2007**, *76*, 064429. [[CrossRef](#)]
5. Moessner, R.; Ramirez, A.P. Geometrical frustration. *Phys. Today* **2006**, *59*, 24. [[CrossRef](#)]
6. Cao, M.; Wang, T.; Shadike, Z.; Nam, K.; Zhou, Y.; Fu, Z. Reversible Multi-Electron Transfer of $\text{Cr}^{2.8+}/\text{Cr}^{4.4+}$ in O_3 -Type Layered $\text{Na}_{0.66}\text{Fe}_{1/3}\text{Cr}_{1/3}\text{Ti}_{1/3}\text{O}_2$ for Sodium-Ion Batteries. *J. Electrochem. Soc.* **2018**, *165*, A565–A574. [[CrossRef](#)]
7. Li, X.; Li, D.; Song, D.; Shi, X.; Tang, X.; Zhang, H.; Zhang, L. Unravelling the Structure and Electrochemical Performance of Li–Cr–Mn–O Cathodes: From Spinel to Layered. *ACS Appl. Mater. Interfaces* **2018**, *10*, 8827–8835. [[CrossRef](#)]
8. Xu, M.; Fei, L.; Zhang, W.; Li, T.; Lu, W.; Zhang, N.; Lai, Y.; Zhang, Z.; Fang, J.; Zhang, K.; et al. Tailoring anisotropic Li-Ion transport tunnels on orthogonally arranged Li-rich layered oxide nanoplates toward high-performance Li-ion batteries. *Nano Lett.* **2017**, *17*, 1670–1677. [[CrossRef](#)]
9. Benedek, R.; Iddir, H. Simulation of First-Charge Oxygen-Dimerization and Mn-Migration in Li-Rich Layered Oxides $x\text{Li}_2\text{MnO}_3 \cdot (1-x)\text{LiMO}_2$ and Implications for Voltage Fade. *J. Phys. Chem. C* **2017**, *121*, 6492–6499. [[CrossRef](#)]
10. Chisholm, M.H.; Eilerts, N.W.; Huffman, J.C.; Iyer, S.S.; Pacold, M.; Phomphrai, K. Molecular design of single-site metal alkoxide catalyst precursors for ring-opening polymerization reactions leading to polyoxygenates. 1. Polylactide formation by achiral and chiral magnesium and zinc alkoxides, ($\eta^3\text{-L}$)MOR, where L = trispyrazolyl- and trisindazolylborate ligands. *J. Am. Chem. Soc.* **2000**, *122*, 11845–11854.
11. Ovitt, T.M.; Coates, G.W. Stereoselective ring-opening polymerization of rac-lactide with a single-site, racemic aluminum alkoxide catalyst: Synthesis of stereoblock poly(lactic acid). *J. Polym. Sci. A Polym. Chem.* **2000**, *38*, 4686–4692. [[CrossRef](#)]
12. Mishra, S.; Agarwal, R.; Singh, A. Four novel classes of heterobimetallic isopropoxides of chromium(III). *Transit. Met. Chem.* **2002**, *27*, 712–715. [[CrossRef](#)]
13. Agarwal, S.K.; Mehrotra, R.C. Synthesis and physico-chemical studies of bimetallic alkoxy derivatives of chromium(III) with niobium(V) and tantalum(V). *Inorganica Chim. Acta* **1986**, *112*, 177–181. [[CrossRef](#)]
14. Mahendra, K.N.; Mehrotra, R.C. Preparation and Reactions of Chromium(III) alkoxides. *Synth. React. Inorg. Met.-Org. Chem.* **1990**, *20*, 963–973. [[CrossRef](#)]
15. Brown, D.A.; Cunningham, D.; Glass, W.K. Studies of chromium(III) alkoxides. *J. Chem. Soc. A* **1968**, *0*, 1563–1568. [[CrossRef](#)]
16. Edema, J.J.; Gambarotta, S.; Smeets, W.J.; Spek, A.L. Polymetallic chromium alkoxides: Synthesis and crystal structures of $(\text{iso-PrO})_8\text{Cr}_2\text{Na}_4(\text{THF})_4$ and $(\mu_3\text{-OPh})_{10}\text{Cr}_4(\mu_3\text{-O})_3\text{Na}_4(\text{TMEDA})_4$. *Inorg. Chem.* **1991**, *30*, 1380–1384. [[CrossRef](#)]
17. Tóth, S.; Wehinger, B.; Rolfs, K.; Birol, T.; Stuhr, U.; Takatsu, H.; Kimura, K.; Kimura, T.; Rønnow, H.M.; Rüegg, C. Electromagnon dispersion probed by inelastic X-ray scattering in LiCrO_2 . *Nat. Commun.* **2016**, *7*, 13547. [[CrossRef](#)]
18. Garg, A.; Errandonea, D.; Pellicer-Porres, J.; Martinez-Garcia, D.; Kesari, S.; Rao, R.; Bettinelli, M. LiCrO_2 Under Pressure: In-Situ Structural and Vibrational Studies. *Crystals* **2019**, *9*, 2. [[CrossRef](#)]
19. Feng, G.X.; Li, L.F.; Liu, J.Y.; Liu, N.; Li, H.; Yang, X.Q.; Huang, X.J.; Chen, L.Q.; Nam, K.W.; Yoon, W.S. Enhanced electrochemical lithium storage activity of LiCrO_2 by size effect. *J. Mater. Chem.* **2009**, *19*, 2993–2998. [[CrossRef](#)]
20. Zopes, D.; Hegemann, C.; Schläfer, J.; Tyrra, W.; Mathur, S. Single-Source Precursors for Alloyed Gold–Silver Nanocrystals—A Molecular Metallurgy Approach. *Inorg. Chem.* **2015**, *54*, 3781–3787. [[CrossRef](#)]
21. Garg, R.; Hegemann, C.; Mathur, S. Heterobimetallic Alkoxides $[\text{Cd}^{\text{II}}\text{M}^{\text{V}}(\text{O}i\text{Pr})_7]_2$ (M = Nb, Ta) as Potential Precursors to Pyrochlore $\text{Cd}_2\text{M}_2\text{O}_7$. *Eur. J. Inorg. Chem.* **2017**, *2017*, 3383–3389. [[CrossRef](#)]
22. Jamil, A.; Schläfer, J.; Gönüllü, Y.; Lepcha, A.; Mathur, S. Precursor-derived rare earth metal pyrochlores: $\text{Nd}_2\text{Sn}_2\text{O}_7$ nanofibers and thin films as efficient photoabsorbers. *Cryst. Growth Des.* **2016**, *16*, 5260–5267. [[CrossRef](#)]
23. Barley, H.R.L.; Kennedy, A.R.; Mulvey, R.E. A mixed iron(III)/lithium alkoxide. *Acta Crystallogr. C* **2005**, *61*, m346–m347. [[CrossRef](#)] [[PubMed](#)]
24. Mäntymäki, M.; Ritala, M.; Leskelä, M. Double metal alkoxides of lithium: Synthesis, structure and applications in materials chemistry. *Coord. Chem. Rev.* **2012**, *256*, 854–877. [[CrossRef](#)]

25. Bonomo, R.P.; Di Bilio, A.J.; Riggi, F. EPR investigation of chromium(III) complexes: Analysis of their frozen solution and magnetically dilute powder spectra. *Chem. Phys.* **1991**, *151*, 323–333. [[CrossRef](#)]
26. Bradley, D.C. Metal alkoxides as precursors for electronic and ceramic materials. *Chem. Rev.* **1989**, *89*, 1317–1322. [[CrossRef](#)]
27. Ojelere, O.; Graf, D.; Ludwig, T.; Vogt, N.; Klein, A.; Mathur, S. Reductive transformation of V(III) precursors into vanadium(II) oxide nanowires. *Dalton Trans.* **2018**, *47*, 6842–6849. [[CrossRef](#)]
28. McIlvried, K.E.; McCarthy, G.J. *ICDD: 24-0600*; Penn State University, University Park: State College, PA, USA, 1972.
29. Herres, N.; Klapper, H. *ICDD: 31-0715*; Institut for Kristallographie, Technische Hochschule: Aachen, Germany, 1979.
30. Tanaka, M.; Kageyama, T.; Sone, H.; Yoshida, S.; Okamoto, D.; Watanabe, T. Synthesis of Lithium Metal oxide nanoparticles by induction thermal plasmas. *Nanomaterials* **2016**, *6*, 60. [[CrossRef](#)]
31. *X-AREA*; Stoe & Cie GmbH: Darmstadt, Germany, 2005.
32. *X-RED32, 1.31*; Stoe & Cie GmbH: Darmstadt, Germany, 2005.
33. *X-SHAPE, 1.06*; Stoe & Cie GmbH: Darmstadt, Germany, 1999.
34. Farrugia, L.J. WinGX suite for small-molecule single-crystal crystallography. *J. Appl. Cryst.* **1999**, *32*, 837–838. [[CrossRef](#)]
35. Altomare, A.; Cascarano, G.; Giacovazzo, C.; Guagliardi, A.; Burla, M.C.; Polidori, G.; Camalli, M. SIRPOW. 92—A program for automatic solution of crystal structures by direct methods optimized for powder data. *J. Appl. Cryst.* **1994**, *27*, 435. [[CrossRef](#)]
36. Sheldrick, G.M. A short history of *SHELX*. *Acta Cryst. A* **2008**, *64*, 112–122. [[CrossRef](#)] [[PubMed](#)]
37. Spek, A.L. Single-crystal structure validation with the program PLATON. *J. Appl. Cryst.* **2003**, *36*, 7–13. [[CrossRef](#)]



© 2019 by the authors. Licensee MDPI, Basel, Switzerland. This article is an open access article distributed under the terms and conditions of the Creative Commons Attribution (CC BY) license (<http://creativecommons.org/licenses/by/4.0/>).